Energy & Environmental Science

Accepted Manuscript

ROYAL SOCIETY OF CHEMISTRY

www.rsc.org/ees

Journal Name

ARTICLE

Nickel Selenide As High-efficiency Catalyst for Oxygen Evolution Reaction

Received 00th January 20xx,
Accepted 00th January 20xx

DOI: 10.1039/x0xx00000x

www.rsc.org/

A. T. Swesi,[#] J. Masud[#] and M. Nath*

A metal-rich form of Ni-selenide, Nickel subselenide, Ni_3Se_2 has been investigated as a potential oxygen evolution electrocatalyst in alkaline conditions for the first time. The Ni_3Se_2 phase has a structure similar to the sulfur mineral *Heazlewoodite*, which contains metal – metal bonding. The electrocatalytic activities of Ni_3Se_2 towards OER was seen to be at par with or even superior to the transition metal oxide based electrocatalyst in terms of onset overpotential for O_2 evolution as well as overpotential to reach a current density of 10 mA/cm^2 (observed at 290 mV). The electrocatalytic Ni_3Se_2 films were grown by electrodeposition on conducting substrates and the deposition parameters including pH of the electrolytic bath, deposition potential, and substrate composition were seen to have some influence on the catalytic activity. So far, Ni_3Se_2 films deposited on Au-coated Si substrate was seen to have the lowest overpotential. Annealing of the *as-deposited* electrocatalytic films in an inert atmosphere, enhanced their catalytic efficiencies by decreasing the overpotential (@ 10 mA/cm^2) as well increasing the current density. The structure and morphology of these films has been characterized with powder X-ray diffraction, Scanning and Transmission electron microscopy, Raman, and X-ray photoelectron spectroscopy. Catalytic activities were investigated through detailed electrochemical studies under alkaline conditions, including linear sweep voltammetry, chromoamperometric studies at constant potential, electrochemical surface area determination and calculating Tafel slope. Faradaic efficiency of this catalyst has been estimated by reducing the evolved O_2 in a RRDE set-up which also confirmed that the evolved gas was indeed O_2. In addition to low overpotentials, these Ni_3Se_2 electrodeposited films were seen to be exceptionally stable under conditions of continuous O_2 evolution for extended period (42h).

1 Introduction

The splitting of water into H_2 and O_2 through application of sunlight or electric pulse has been an attractive avenue for alternative energy generation using earth abundant resources for the last several decades.[1-3] The efficiencies of oxygen and hydrogen evolution reactions (OER and HER, respectively) which are the constituent half reactions for water splitting play a critical role in the advancement of renewable energy technologies like metal-air batteries or solar-to-fuel energy production. Among these, although the oxygen evolution reaction has the advantages of being sustainable and relatively benign in terms of impact on the environment and human health, however, OER typically being a 4 electron process requiring O – O bond formation is a kinetically slow process.[4] Several catalysts are normally used to expedite this inherently sluggish process by reducing the overpotential (η) at the respective electrode and also by increasing the rate of conversion.[5-13] The primary considerations for designing an efficient OER catalyst includes long term stability under corrosive conditions of oxygen evolution, low cost, and widely available materials together with a low overpotential.[9,10,14] To date some of the most efficient and robust OER catalysts in acidic or alkaline medium are based on precious metal oxides like IrO_2 and RuO_2.[9,15,16] However, these precious metal oxides are not the most economically viable options for these catalytic processes based on cost considerations and scarcity of raw materials. The incessant search for efficient OER catalysts from earth abundant materials have resulted in identification of several transition metal based oxides as efficient OER catalyst with low η, some of them being comparable with the IrO_2 and RuO_2 catalysts. In particular, Ni and its oxides/hydroxides have long been studied for OER electrocatalytic activities in alkaline solution since last century primarily due to their enhanced catalytic activity, stability in alkaline solutions and low cost of Ni.[17-30] Merrill and Dougherty assessed a series of transition metal (Mn – Cu) oxide as electrocatalysts for the electrolysis of water.[31] Among this group, a Ni-Fe oxide mixture was found as

[a] *Department of Chemistry, Missouri S&T, Rolla, MO 65409.*
* E-mail: nathm@mst.edu.
# These authors contributed equally to this work.
Electronic Supplementary Information (ESI) available: Pxrd patterns of Ni_3Se_2 deposited at different pH; XPS spectra for O; LSV plots from Ni_3Se_2 for 100 cycles in unpurified and purified KOH; LSV and constant potential plots from Ni_3Se_2 films after 2 days of chronoamperometry; SEM images of the annealed Ni_3Se_2 films; EDS line scan analysis and mapping for the films; pxrd patterns of the annealed Ni_3Se_2 films; O1s and Se 3d XPS signals before and after OER; Raman spectra after 2d of chronoamperometry; thickness analyses of the electrodepoited film with 3D digital imaging; variation of the onset potential with catalyst loading; Elemental analyses through EDS before and after annealing. See DOI: 10.1039/x0xx00000x

the optimum catalyst and it was stated that the catalytic properties of the metal oxides can be influenced through other variables of the electrodeposition reaction such as the total and relative concentration(s) and composition(s) of dissolved metal salts and extra electrolytes, the pH, and the duration of the electrodeposition current. Even though in recent times, the most efficient catalytic activity towards OER was obtained by using nickel oxides or hydroxides,[19-29] transition metal chalcogenides (ME_n, M = Fe, Co, Ni; *E* = S, Se) have also been investigated as OER, HER, and ORR electrocatalysts.[32-34] Conventionally, transition metal chalcogenides due to their interesting electronic and optical properties,[35] has been extensively used for several high-tech applications, including high-temperature super-conductors,[36,37] photovoltaics,[38] and heterogeneous catalysts.[39] In addition their promising activity towards electrocatalysis,[17,40,41] has made these materials especially attractive for advanced energy related applications. Recently a composite electrode containing Ni_3S_2 nanorods synthesized on Ni foam by hydrothermal reaction exhibited very good catalytic activity for OER with low onset overpotential of ~157 mV in alkaline solutions.[34] In a separate study NiSe nanostructures were shown to have good catalytic activities for HER process.[42] In fact, these recent results illustrate that these transition metal chalcogenides due to their unique electronic configuration and comparatively high catalytic activity, can be promising substitutes for the Pt-based electrocatalysts when their comparable catalytic activities toward the ORR and HER and much lower cost are considered.[40-49] However, more progress is still needed in order to reduce the cost and improve activity and stability of these electrocatalysts.

The promising OER electrocatalytic activities of nickel based compounds[19-34] including nickel sulfide,[34] and the expectation that increasing covalency might lead to better catalytic activities,[5,11] motivated us to investigate the catalytic activity of nickel selenide towards OER reactions. According to Horn and Goodenough's prediction, increased covalency of the metal – oxygen bond in the oxide electrocatalysts leads to better catalytic efficiency.[11] In this article we report a new nickel selenide based electrocatalyst (Ni_3Se_2) which enhances oxygen evolution with high efficiency in alkaline conditions and exhibits exceptional stability for prolonged time under continuous potentiostatic electrolysis conditions. Typically the efficiencies of OER electrocatalysts are benchmarked by measuring the overpotential (η) at which a 10 mA/cm^2 current density is achieved from the oxygen evolution reaction. For the Ni_3Se_2 electrocatalysts reported here, we observed that it can generate 10 mA/cm^2 at overpotential as low as 290 mV (upon annealing or using Au-coated Si as growth substrate) which is one of the lowest overpotentials observed amongst the known OER catalysts, even better that RuO_2, IrO_2 and NiO_x, some of the best performing catalysts. It is interesting to note that this new electrocatalyst can effectively catalyze the OER without any additional modification (such as doping or hybridizing with graphene or noble metals). The Ni_3Se_2 was electrodeposited on different conducting substrates including Au-coated glass, Au-coated Si, glassy carbon (GC), ITO-coated glass, and Ni foam. Detailed structural, morphological and electrochemical characterizations of these Ni-Se based OER catalysts has been carried out, which shows the OER activity was influenced by electrodeposition parameters including deposition time and pH of the electrochemical bath, annealing, and the nature of the substrate.

2 Experimental & Methods

2.1 Electrodeposition of Ni_3Se_2

Nickel acetate tetrahydrate [$Ni(C_2H_4O_2)_2.4H_2O$ from J. T. Baker Chemical Company, USA], Selenium dioxide (SeO_2) [Acros Chemicals], Lithium chloride (LiCl) [Aldrich] and KOH [Fisher Chemicals] were all of analytical grade purity and were used without further purification. Au-coated glass and Au-coated Si used as substrates in electrodeposition was purchased from Deposition Research Lab Incorporated (DRLI), Lebanon Missouri. The FTO- and ITO-coated glass slides were purchased from Fisher scientific. All solutions were prepared using deionized (DI) water with a resistivity of 18 MΩ·cm. Prior to electrodeposition, the substrates were cleaned by ultrasonic treatment in micro-90 followed by isopropanol rinse for three times and eventually rinsed with deionized water (15 min each step) to ensure the clean surface. Au-coated glass/Au-coated Si /ITO-coated glass /FTO-coated glass plates were covered with a Teflon tape, leaving an exposed geometric area of 0.283 cm^2, and connected as the working electrode. Ni_3Se_2 was electrodeposited on the substrate by a controlled-potential deposition at -0.80 V (*vs* Ag/AgCl) for 40, 130, 300, and 600 s from an aqueous solution containing 10 mM $Ni(CH_3CO_2)_2{\cdot}4H_2O$, 10 mM SeO_2 and 25 mM LiCl at 25^{o}C. The pH of the electrolytic bath was adjusted with dilute HCl to be in the range 2.5 - 4.5. After electrodeposition, the substrates were washed with deionized water in order to remove impurities and adsorbents from the surface.

2.2 Annealing of the Ni_3Se_2 films

To investigate the effect of temperature on the catalytic activities, the *as-deposited* films were subjected to thermal annealing in presence of N_2 at 300 °C for 5 - 30 min. Annealing experiments were performed either inside a tube furnace under constant N_2 flow controlled by a mass flow controller (300 °C for 5 min), or in a closed flask under rapid flow of N_2 (300 °C for 30 min).

2.3 Methods of Characterization

Powder X-ray Diffraction: The electrodeposited substrates were studied as such without any further treatment. The product was characterized through powder X-ray diffraction (pxrd) with Philips X-Pert using CuKα (1.5418Å) radiation. Pxrd pattern was collected from the as-synthesized product spread on the growth substrate. Because the product formed a very

thin layer on the substrate, the pxrd was collected at grazing angles in thin film geometry (GI mode with Göbel mirrors).

Scanning and Transmission Electron Microscopy (SEM, TEM): SEM image of the modified electrode surfaces was obtained using a FEI Helios NanoLab 600 FIB/FESEM at an acceleration voltage of 10 kV and a working distance of 4.8 mm. Energy dispersive spectroscopy (EDS) along with line scan analysis was also obtained from the SEM microscope. FEI Tecnai F20 was used to obtain high resolution TEM images (HRTEM) and selected area electron diffraction (SAED) patterns of the catalyst. The probe current is 1.2 nA with a spot size of less than 2 nm. STEM mode in the TEM was also used for dark field imaging where the convergence angle was 13 mrad and the camera length was 30 mm. This scope is equipped with an Oxford ultra-thin (UTW) window EDS detector, which allows detection of the elements. For TEM studies a formvar coated Cu grid was positioned and immobilized on the electrode surface (mainly through capillary action) such that during electrodeposition, some material also deposited on the Cu grid directly, which was then analysed in the TEM.

X-ray Photoelectron Spectroscopy (XPS): XPS measurements of the catalysts were performed by KRATOS AXIS 165 X-ray Photoelectron Spectrometer using monochromatic Al X-ray source. The spectra were collected *as is* and after sputtering with Ar for 2 min which removes approximately 2 nm from the surface.

ICP-MS Analysis: Known quantities of solid samples were digested by 1.5 mL of concentrated optima-grade nitric acid. After digestion, the samples were diluted appropriate times (10 to 100 times for Fe and 100 to 100 times for Ni) and analyzed by ICP-MS method. A NexION 350D ICP-MS (PerkinElmer, Inc. Shelton, CT) was used for the analysis. The ICP-MS was operated in kinetic energy discrimination (KED) mode to minimize polyatomic interferences. Quantitation isotopes included ^{57}Fe and ^{60}Ni. The sampling system was cyclonic spray chamber with a Meinhard nebulizer, sampler and skimmer are platinum cones. ICP-MS operational parameters include: RF power, 1600 W; plasma gas flow, 18 L/min; auxiliary gas flow, 1.20 L/min; KED mode gas flow 4.5 mL/min; and nebulizer gas flow: 1.05 L/min. US EPA method 200.8 quality control guideline was closed followed to insure the high quality data.

Raman Spectra: Horiba Jobin Yvon Lab Raman ARAMIS model was used to perform Raman microspectroscopy on the *as-deposited* catalyst films. The laser used was He-Ne with a power of about 1.7 mW over a range of 100 – 2000 cm^{-1}. The spectra were iterated over an average of 25 scans.

2.4 Electrochemical Characterization and Catalytic Studies:

The OER catalytic performance was estimated from linear scan voltammetry (LSV) plots while the stability of the catalyst was studied by chronoamperometry. Electrochemical measurements were performed in a three-electrode system with an IviumStat potentiostat using Ag/AgCl and Pt mesh as reference and counter electrodes, respectively. All measured potentials *vs* the Ag/AgCl were converted to the reversible hydrogen electrode (RHE) scale *via* Nernst equation (eq. 1):

$$E_{RHE} = E_{Ag/AgCl} + 0.059\ pH + E^{o}_{Ag/AgCl} \quad (1)$$

where E_{RHE} is the converted potential vs. RHE, $E_{Ag/AgCl}$ is the experimentally measured potential against Ag/AgCl reference electrode, and $E^{o}_{Ag/AgCl}$ is the standard potential of Ag/AgCl at 25 ^{o}C (0.197 V). For most of the electrochemical characterizations, the electrode area of the film surface was kept constant at 0.283 cm^2.

Faradaic efficiency of the Ni_3Se_2 catalytic films were estimated from the ORR-OER studies performed with bipotentiostat mode of the IviumStat using a RRDE set-up where GC and Pt were used as a disk and ring electrode, respectively. Ni_3Se_2 was deposited on interchangeable GC disk electrode for 300 s at cathodic potential of -0.80 V *vs* Ag/AgCl. Pt ring was polished with Alumina slurry (0.05 µm), then washed and sonicated in DI water for 5 min. Before the measurements, Pt ring was electrochemically cleaned in N_2 saturated 0.5 M H_2SO_4 until reproducible characteristic CVs of Pt was obtained. The disk electrode containing the electrocatalyst was held at the open circuit potential of OER where no Faradaic process occurs, while the Pt ring electrode was maintained at 0.2 V vs RHE to get the background current of the ring electrode. The background ring current was lower than 20 µA. Then, the voltage of disk electrode was held at several definite potentials in the OER kinetic region for 30 sec, while, the ring current was recorded at 0.2 V *vs.* RHE.

Calculation of the Turnover Frequency (TOF):

The turnover frequency (TOF) was calculated from the following equation (eq. 2):

$$\text{TOF} = \frac{I}{4 \times F \times m} \quad (2)$$

Where *I* is the current in Amperes, *F* is the Faraday constant and *m* is number of moles of the active catalyst.

Tafel plots: The catalytic performance of the Ni3Se2 catalysts toward the OER have been carried out by measuring the Tafel plots based on the equation given below:

$$\eta = a + \frac{2.3\ RT}{\alpha nF} log(j) \quad (3)$$

where η is the overpotential, *j* is the current density and the other symbols have their usual meanings.

The Tafel equation as shown Eq. (3) is a fundamental equation which acquires from the kinetically control region of OER, and relates the overpotential η with the current density *j* where the Tafel slope is given by 2.3RT/αnF. To calculate Tafel slopes, LSV plots were obtained with slow scan speed (2 mV.s^{-1}) in non-stirred solution.

3.0 Results & Discussions

3.1 Structural and Morphological Characterization

The pxrd patterns of as-synthesized films deposited on Au-coated glass substrates showed peaks which could be matched with Ni_3Se_2 phase (JCPDS # 019-0841) along with peaks characteristic of Au arising from the underlying substrate as shown in Figure 1. It was observed that as the deposition time

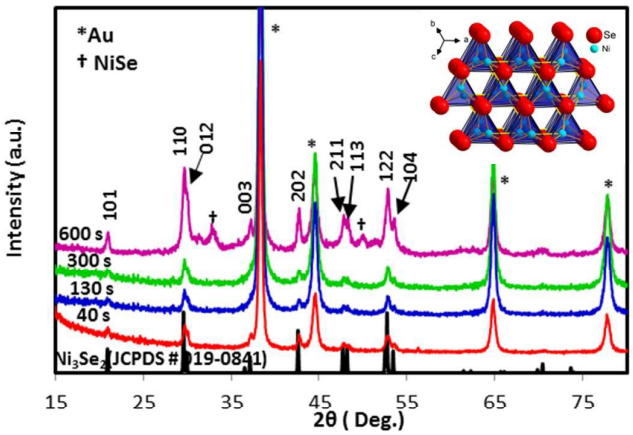

Fig. 1 PXRD patterns of catalysts electrodeposited for different times showing the presence of Ni_3Se_2 (JCPDS # 019-0841) along with Au. Inset shows the crystal structure of Ni_3Se_2 with Ni – blue and Se – red.

increased the crystallinity of the deposited film was enhanced as depicted by the increasing intensity of the pxrd peaks. With very long deposition times (600 s), however, trace amounts of NiSe (JCPDS # 03-065-9451) could be detected in the films from their pxrd patterns. Almost identical phase of nickel selenide (Ni_3Se_2) was observed in catalysts deposited at different pH of the electrochemical bath (2.5, 3.5, and 4.5) as shown in supplementary Figure S1 with the film deposited at pH 2.5 showing the best pattern. Hence, catalyst used in rest of the study was synthesized at pH 2.5. Ni_3Se_2 has a structure very similar to the sulfide analogue, Ni_3S_2, also known as *heazlewoodite*, which is a sulfur-poor nickel sulfide mineral.[50,51] *Heazlewoodite* contains Ni in a distorted tetrahedral environment with short Ni - Ni distances suggestive of metal-metal bonds. From local energy density studies it has been predicted that Ni - chalcogen and Ni - Ni bonds are intermediate in character between ionic and covalent.[52,53] Unlike Ni_3S_2, detailed structural studies on Ni_3Se_2 are still rare. However, in analogy with the sulfide phase, it has been shown that Ni_3Se_2 also have Ni-Ni bonding in the structure with one of the Ni-Ni bonds being very short and similar to that found in metallic Ni.[54] The structure of Ni_3Se_2 has been shown in the inset of Figure 1.‡

Detailed SEM studies of the as-deposited films showed that the films were mainly granular and composed of nano-structured grains (50 nm to several hundred nm) (Figure 2a). It was clear that the Ni_3Se_2 grain size increased with increasing deposition time from 40 s to 600 s and the films grow thicker, but smoother with the time (Supplementary Figure S2a). Typically the average thickness of the films varied between 0.9 – 5.2 µm (Table ST1 in supplementary information). The amount of catalyst loading was also estimated from analyzing the electrodeposition curves (*vide infra,* Table 1) and the results show that the catalysts amount as well as loading per unit area increased with increasing deposition time. EDS was used to measure the elemental compositions and the Ni to Se atomic ratios in these catalysts, and the results are shown in Figure 2b and supplementary Figure S2b. Typically SEM performed on a wide area of the film showed uniform presence of Ni and Se, as evident by the line scan analyses showin in supplementary Figure S2b(i). SEM was also performed in STEM mode with HAADF (high angle annular dark field) imaging on individual grains which again showed that Ni and Se were present uniformly in individual grains and the distribution was similar to that obtained in the film (supplementary Figure S2b(ii)). The Ni:Se atomic ratio for the catalysts synthesized at 40 and 130 s is slightly higher than the theoretical atomic ratio of Ni_3Se_2 (1.5) whereas at 300 and 600 s of electrodeposition, the Ni:Se ratio were closer to the theoretical value. It should be noted that the relative atomic percentage of Se increased with increasing deposition time, which might be due to the competing deposition of Ni and Se during co-electrodeposition, as the metal chalcogenide process is known to be partially controlled by the diffusion of chalcogen ions to the cathode.[55] The deviation of the Ni:Se elemental ratio from theoretical value of 1.5 might still be advantageous for enhancing the catalytic activity even further in the Se-deficient (i.e. Ni-rich) compositions.[56] Typically for the Ni-oxide based catalysts, it was observed that creation of anion deficiency improved catalytic performance.[9,11]

Elemental compositions of the electrodeposited films were also investigated through XPS studies. The XPS spectrum of the catalysts (Figure 2c) exhibits two peaks at 852.6 and 869.8 eV, corresponding to Ni $2p_{3/2}$ and Ni $2p_{1/2}$ similar to that obtained from Ni_3S_2.[57,58] It should be noted that the binding energies for these peaks were more shifted towards the binding energies observed in metallic or alloyed Ni, as would be expected for Ni_3Se_2 which has substantial metal-metal bonding. In films deposited for 600 s, another set of very weak intensity Ni 2p peaks were observed at 856.1 and 873.6 eV, which corresponds to Ni $2p_{3/2}$ and Ni $2p_{1/2}$ for NiSe and is also closer to the Ni-O phases.[59] Accordingly XPS was collected to detect O. Some surface oxygen was detected (supplementary figure S3) that reduced in intensity following sputtering for 2 min under Ar, indicating that the impurity phase was mostly on the surface. These XPS results along with XRD confirmed that the majority phase in these electrodeposited films was Ni_3Se_2. An obvious satellite was observed at higher energy of the Ni 2p peak (about 860.0 eV) which could be due to the antibonding orbital between the Ni atom and Se atom. Similar satellite peaks has been reported for several Ni-based chalcogenides.[60] The binding energies of $3d_{5/2}$ levels of Se were obtained at 54.7 eV similar to the that from nickel selenides.[61]

The film morphology was also analyzed through TEM and HRTEM imaging which showed crystalline nature of the granules in the film, with lattice fringes corresponding to <110> lattice spacing of Ni_3Se_2 (Figure 2d). The SAED pattern shown as inset of Figure 2d, also confirmed crystalline nature of the as-prepared films and the diffraction spots could be indexed to <101> and <110> lattice planes of Ni_3Se_2.

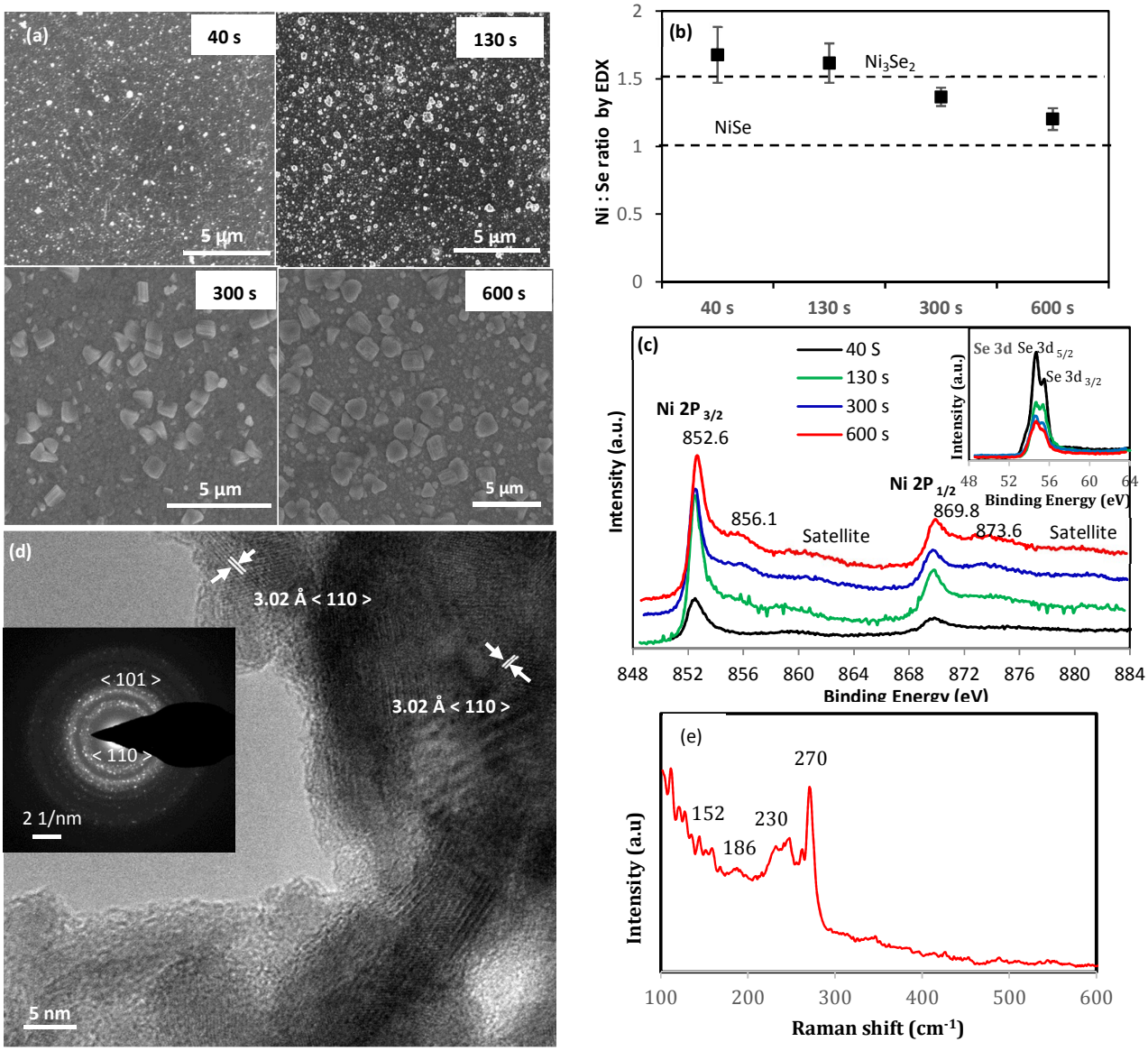

Fig. 2 (a) SEM images of catalyst deposited for 40, 130, 300 and 600 s. (b) Ni to Se ratio obtained from the catalysts through EDS. Dotted lines represent the ratio lines for NiSe(bottom) and Ni_3Se_2 (top) phases. (c) XPS spectra of the catalyst showing the Ni 2p peaks. Inset shows peaks corresponding to Se 3d. (d) HRTEM image of the catalyst. Inset shows typical SAED pattern. (e) Raman spectrum of the catalyst electrodeposited for 300 s.

Raman spectrum of the as-synthesized catalyst for 300 s is shown in Figure 2e. There are four Raman peaks at 152, 186, 230 and 270 cm^{-1} which can be assigned to the Raman active modes of Ni_3Se_2.[62] There is no evidence of elemental Se in catalyst, as no peaks were observed at 141 and 235 cm^{-1}. The Raman analysis also did not show major presence of any oxidic phases further confirming that the electrodeposited films were devoid of oxidic impurities.

3.2 Electrochemical Performance and OER Catalytic Activities

The electrocatalytic performance for OER of the electrodeposited films was investigated through detailed electrochemical studies in alkaline solution (0.3M KOH) near pH 13. The electrochemically active surface areas (ECSA) of the catalysts were estimated by measuring the electrochemical capacitance of the electrode-electrolyte interface in the double-layer regime of the voltammograms. Using N_2-saturated 0.3 M KOH, the electrode was potentiostatically cycled from -0.19 to -0.10 V vs Ag/AgCl at scan rates between 2.5 and 40 mV s^{-1} (Figure 3). The capacitive current (i_{DL}) was estimated from the non-faradaic double-layer region. This current involves charge accumulation rather than chemical reactions or charge

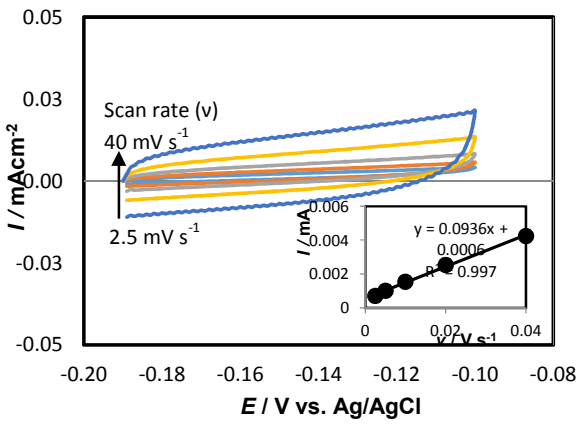

Fig. 3 Cyclic voltammograms measured for Ni_3Se_2 catalyst (electrodeposited for 300 s) in N_2 saturated 0.3 M KOH solution at different scan rate from 2.5 to 40 mV s^{-1}. Inset shows plot of anodic current measured at -0.14 V as function of scan rate.

transfer and is directly proportional to the scan rate, v (V/s) as shown in eq. 4:[9]

$$i_{DL} = C_{DL} * v \quad (4)$$

where C_{DL} is the specific capacitance of the electrode double layer (F/cm^2 electrode).

Thus, a plot of i_{DL} against v shown in the inset of Figure 3 gave a straight line and the slope was equal to C_{DL}. Hence, the ECSA of catalyst was calculated as (eq. 5):

$$ECSA = C_{DL} / C_s \quad (5)$$

C_s is the specific capacitance and reported to be between 0.022 to 0.130 mF cm^{-2} in alkaline solution. In this study, we use the value of C_s is 0.040 mF cm^{-2} based on previously reported Ni-based OER catalysts.[9] The ECSA and the roughness factor (RF) of the various catalysts used in this study are given in Table 1. It was observed that RF became less as the film deposition time increased which corroborated with the fact that the films looked thicker and smoother with increasing deposition time.

To study the electrocatalytic activity of the Ni_3Se_2 for OER, liner sweep voltammetry (LSV) measurements were conducted in N_2-saturated 0.3 M KOH, at a scan rate of 10 mV s^{-1}. To the best of our best knowledge, this is the first time that Ni_3Se_2 has been reported as an OER-active electrocatalyst. Figure 4a shows the LSVs of electrochemical oxygen evolution with Ni_3Se_2 catalysts deposited for 40, 130, 300 and 600 s. Typically rapid oxygen evolution from the Ni_3Se_2 catalyst surface was observed during the electrochemical studies. As observed, blank Au shows poor catalytic activity toward the OER. In contrast, after electrodeposition of Ni_3Se_2 the substrates showed high activity for OER with an onset overpotential of about 210 mV for 300 s, 220 mV for 40, 130 s deposition and 250 mV for 600 s deposition, respectively [all potentials have been reported with respect to RHE]. This ~30 mV shift in onset overpotential is expected as longer time (600 s) leads to bulk deposition of catalyst (Table 1). Conventionally, the effectiveness of OER catalysts are estimated by listing the overpotential required to reach a current density of 10 mA/cm^2 (per geometric surface area), which is considered to be equivalent to 10 % solar energy conversion efficiency.[9] The η for 10 mA/cm^2 per geometric area of the Ni_3Se_2 catalysts electrodeposited for different times are reported in Table 1. It can be clearly found that the 300 s deposited catalyst exhibits the highest catalytic activity towards OER with a much lower η. It should be noted that with increasing deposition time and the increase of Ni_3Se_2 content in composites (Table 1), the catalytic activity for OER increased at first and then decreased (supplementary figure S5). After studying in detail electrochemical and surface specific properties, the authors conclude that this enhanced activity is due to a fine balance between the catalyst loading, surface roughness, thickness of the film, and grain sizes. It can be envisioned that catalyst loading will have a direct influence on the capability of O_2 evolution in the semiconductor-based water oxidation catalysts.[63] Increasing catalyst loading increases the amount of catalytically active sites thereby facilitating the gas evolution reaction. As can be seen from Table 1, the catalyst loading increases with increasing deposition time. However as the thickness of the film increases with deposition time, some of the surface active sites will be blocked by overgrowth and multilayers, thereby reducing access of water molecules to the active sites. Additionally, larger thickness of these semiconductor films also affects mobility of charge carriers and electrical conductivity in the underlying Au layer. In the electrode composites, Ni_3Se_2 film provides catalytically active sites, while underneath Au substrate favors the higher mobility of charge carriers and superior electrical conductivity. Thus, it is reasonable that the catalytic activity gradually increases with the increase in the thickness of Ni_3Se_2 within a certain range. However, when the Ni_3Se_2 thickness is further increased over its optimum value, the catalytic performance deteriorates, which may be due to

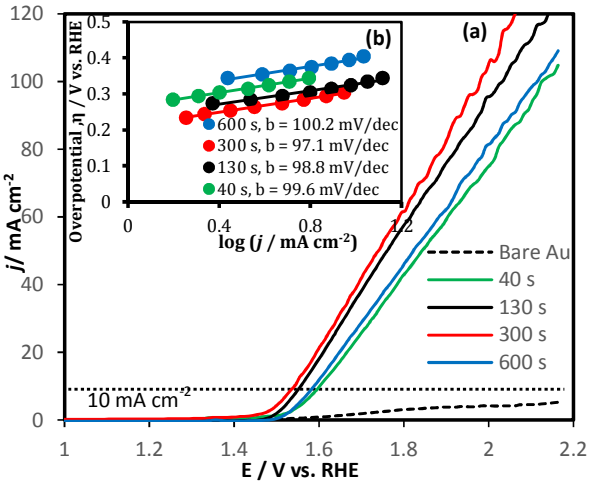

Fig. 4 (a) LSVs measured for catalysts electrodeposited for different times in N_2 saturated 0.3 M KOH solution at a scan rate of 0.01 V s^{-1}. Dotted line shows the current density of 10 mA $cm^{-2.}$ (b)Tafel plots of catalysts.

the lower mobility of charges due to semiconductor chalcogenide. Surface roughness of the film on the other hand, has a positive effect on the catalytic activity. Higher surface roughness (roughness factor) indicates exposure of more surface active sites for catalysis, thereby increasing catalytic efficiency. Thus it is apparent that to maximize catalyst efficiency, one needs to have high catalyst loading with high roughness factor and smaller thickness. From Table 1 it can be seen that the films deposited at 300 s satisfy all these criteria and strike a fine balance between the different parameters. Hence these films show the best catalytic activity among the Ni_3Se_2 films reported here.

It was observed that all the electrocatalysts were stable under the O_2 evolution conditions as revealed by chronoamperometric studies for 3h (Supplementary figure S4). Note that the overpotential required to achieve close to 10 mA/cm^2 of 300 s catalyst (310 mV) is comparable with the widely used OER catalysts, IrO_x (320 mV) and RuO_2 (390 mV).[9, 15] Literature surveys are also showed that among the Ni-based catalysts, our synthesized Ni_3Se_2 catalyst exhibits a lower overpotential at the current density of 10 mA/cm^2 (*vide infra*).

Specific activity is an intrinsic property of catalyst and is important for comparison of the loading of catalyst with varying deposition time. Activities of the OER catalysts were also determined from the specific current density at constant overpotential of 310 mV. The specific current density, j_s, can be calculated from the ratio of the current density per geometric area (j_g) at 310 mV with the roughness factor (RF) of the surface as shown in eq 6.[9]

$$j_s = \frac{j_g}{RF} \qquad (6)$$

The specific current density were measured for different catalysts and shown in Table 1. The highest specific current density at 310 mV overpotential was obtained for 300 s catalyst, indicating that this was indeed best OER catalyst among the Ni_3Se_2 films deposited for various times.

Tafel slopes are another important parameter that offers critical insights into the OER reaction kinetics. The Tafel slopes were collected from the steady-state LSVs at a scan rate of 2 mV s^{-1} in a non-stirred solution. The Tafel plots for Ni_3Se_2 electrodeposited films are shown in Figure 4b. A linear dependency of η *vs* log(j) was achieved for all catalysts and they displayed different slopes. The Tafel slope values are listed in Table 1 and the slopes follow an order of 300 s < 130 s < 40 s < 600 s. The lowest value of Tafel slope indicates facile catalytic activity for OER.

The evolved gas at the anode was analysed with the aid of electrochemical reduction in a bipotentiostat set-up. Typically O_2 can be reduced electrochemically by Pt cathode held at a potential of 0.2 V (vs. RHE). To confirm the composition of the evolved gas, Ni_3Se_2 was deposited on glassy carbon (GC) which was connected as the disk electrode in a RRDE set-up with Pt as the ring electrode. The ring electrode was maintained at a constant potential of 0.2 V (vs. RHE) and the current was recorded (ring current) as the potential of the disk electrode was scanned over a desired range. The electrolyte was purged with N_2 for 30 min before staring the electrochemical oxidation to get rid of any dissolved O_2 and blanketed with N_2 atmosphere. Fig. 5 (a) shows the LSV at GC disk electrode in 0.3 M KOH at 1600 rpm at a scan rate of 10 mV s^{-1} where in absence of dissolved O_2 the ring current is minimal as observed. As the potential of the disk electrode was swept past 220 mV (onset overpotential), the characteristic increase of the cathodic ring current due to ORR indicated that the bubbles formed at the anode were indeed O_2. The ring current progressively increased with increasing potential as more and more O_2 was evolved at the anode. To further confirm that the ring current was indeed from the dissolved O_2 generated *in situ* from the Ni_3Se_2 catalyst, a series of experiments were performed where the disk current was collected after various periods of O_2 generation. The electrolyte was initially purged with N_2 gas for 30 min to get rid of dissolved O_2 and blanketed with N_2 atmosphere during recording the ring current. Then the disk electrode was held at constant 10 mA cm^{-2} current density per geometric area (which was sufficiently large to ensure O_2 generation) for 1, 2 and 6 h in 0.3 M KOH solution following which the ORR currents at Pt ring electrode were measured as shown in Figure 5 (b). It was observed that ORR current increased with time of O_2 generation and after 6 h current was comparable to that obtained from a solution saturated with O_2 externally. To further confirm that the O_2 was obtained *in situ*, the same solution (after generation of O_2 for 6 h) was purged again with N_2 for 2 h to get rid of the evolved O_2, and ORR current was measured which showed that it had reduced back to minimal current as was seen before start of the experiment (black dashed curve in Figure 5b). This proves that the dissolved O_2 was indeed generated *in situ* by the anodic catalyst.

Table 1. Electrochemical parameters of the Ni_3Se_2 catalysts measured in 0.3 M KOH

Deposition time	Total loading / µg	Loading/area / mg.cm^{-2}	Grain sizes /nm	ECSA /cm^2	RF	Onset η / V[a]	η to 10 mAcm^{-2} / V[a]	Tafel slope / mV.dec^{-1}	$j_{g,\ \eta=0.31\ V}$ / mA.cm^{-2}	$j_{s,\ \eta=0.31\ V}$ / mA.cm^{-2}
40 s	8.0	2.83 x 10^{-2}	30-150	2.5	8.8	0.22	0.37	99.6	3.36	0.38
130 s	31.3	11.1 x 10^{-2}	70-200	2.3	8.2	0.22	0.33	98.8	7.81	0.95
300 s	61.4	21.7 x 10^{-2}	150-1500	2.3	8.2	0.21	0.31	97.1	10.24	1.25
600 s	123.4	43.5 x 10^{-2}	300-2000	1.8	6.5	0.25	0.36	100.2	3.88	0.60

[a] potential reported with respect to RHE

The Faradaic efficiency of OER was determined by RRDE, containing 0.3M of KOH following previously reported procedure (supplementary information and figure S6).[9,64] Prior to RRDE measurement, N_2 gas was purged in the cell for 30 min and then blanketed with N_2 during the experiment. The disk electrode was maintained at constant potential steps from 1.48 to 1.56 V (*vs* RHE) for consecutive periods of 1 min each, while being rotated at a 1600 rpm under a N2 gas blanket. The ring electrode was held at 0.2 V (vs. RHE) throughout the experiment, which was sufficiently negative to reduce the collected oxygen rapidly. The Faradaic efficiency can be given as (eq. 7):[9]

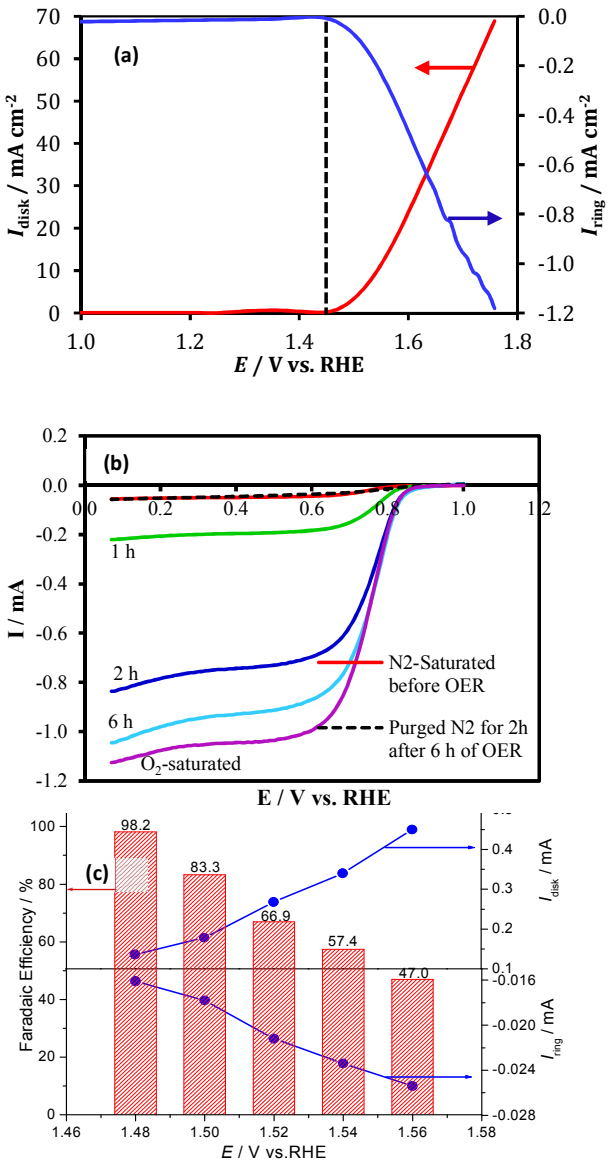

Fig. 5 (a) OER at Ni_3Se_2/GC disk electrode in N_2-saturated 0.3 M KOH and Pt ring current (held at 0.2 V vs. RHE) due to oxygen reduction as a function of disk potential. Black dash line shows the onset of OER at the disk electrode and ORR at the ring electrode. (b) Electrochemical evidence of O_2 generation at the disk electrode and reduction at ring electrode when constant current of 10 mA cm^{-2} was applied at disk electrode for varying periods of time (1, 2 and 6 h) in N_2 saturated and blanketed 0.3 M KOH. (c) Faradaic efficiency of catalyst in 0.3 M KOH at 1600 rpm under N2 saturation. The disk and ring currents of RRDE plotted as function of the applied disk potential along with the calculated Faradaic efficiency.

where oxygen generated at the disk electrode was swept outward away from the disk electrode and towards the Pt ring electrode where it was reduced. The collection efficiency, N (0.24), of the rotating ring-disk electrode was determined by the ratio of ring and disk current in 0.001M $K_3Fe(CN)_6$

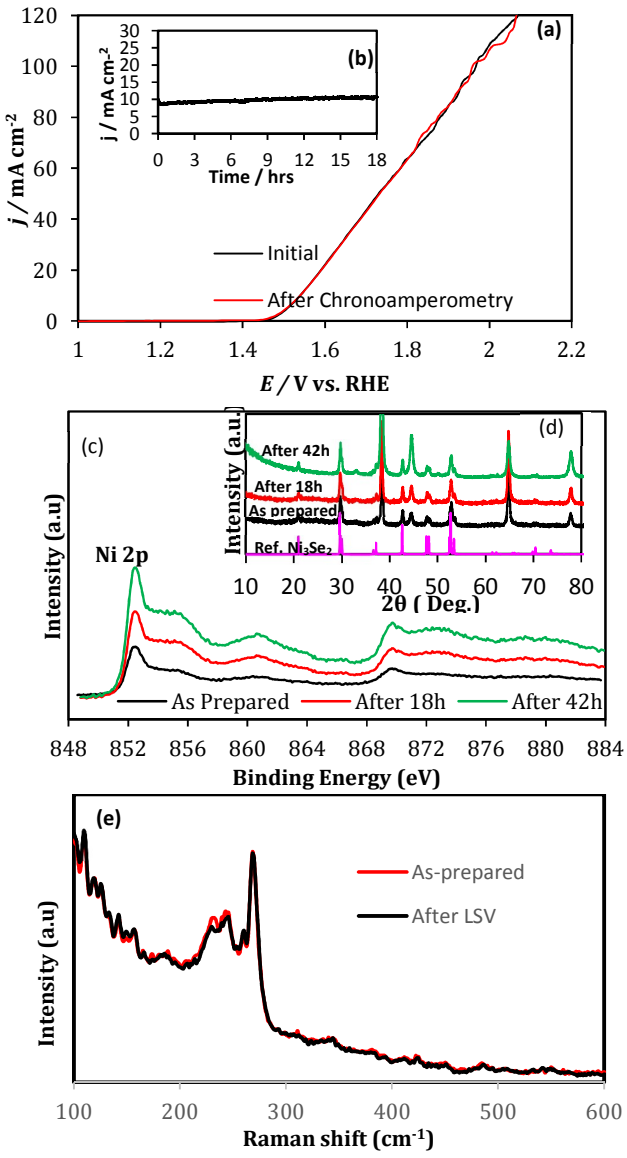

Fig. 6 (a) LSVs of catalyst synthesized for 300 s in N_2 saturated 0.3 M KOH before and after chronoamperometry for 18 h, (b) extended stability study of catalyst under continuous O_2 evolution (at 10 mA/cm2) for 18 h studied through chronoamperometry at constant potential. (c) XPS spectra before and after chronoamperometry for 18 and 42h, and (d) XRD patterns before and after current transient experiment for 18 and 42 h.(e) Comparison of Raman shift before and after LSV for OER.

Faradaic Efficiency = $\frac{2i_r}{i_d N}$ (7)

where i_r and i_d are the measured ring and disk currents, respectively, and N is the collection efficiency of RRDE, 0.24 in this work. Figure 5 (c) shows the plot of the disk and ring currents of Ni_3Se_2 catalyst in 0.3 M KOH as a function of the applied disk potential and Faradaic efficiency. The highest Faradaic efficiency was obtained as about 98% at the applied disk potential of 1.48 V (vs RHE), and decreased to 47% with the disk voltage increasing to 1.56 V (vs RHE). This decrease can be attributed to apparently large amounts of undissolved oxygen bubbles generated at the relatively high applied disk potentials which might not be collected efficiently by the Pt ring electrode. This decrease in Faradaic efficiency has been observed by other researchers also with Ni-Fe based nanoparticle electrocatalysts in alkaline medium.[64] Thus, the 98% Faradaic efficiency which was achieved at 1.48 V (vs RHE) (corresponding to about 1.0 mA cm^{-2} disk current density), has been presented as the OER efficiency of the Ni_3Se_2 catalyst because this disk current density is adequately high to generate oxygen.

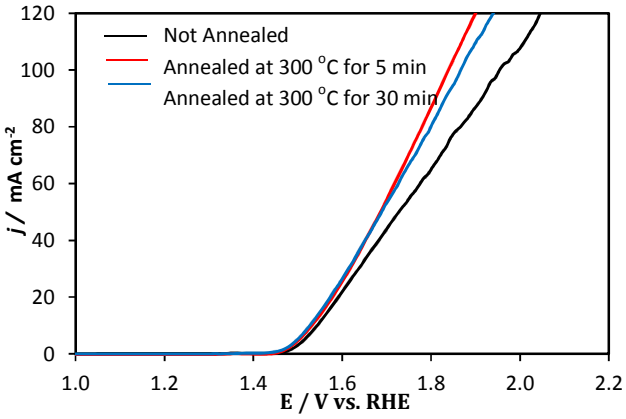

Fig. 7 Comparison of LSVs measured before and after annealing at 300 °C for 5 min and 30 min of catalyst in 0.3 M KOH solution at 0.01 V s^{-1}.

The turnover frequency (TOF) of the Ni_3Se_2 catalyst deposited for 300 s, was calculated at an overpotential of 300 mV in 0.3 M KOH, assuming all of the active materials in the catalysts are catalytically active for OER, and using the catalyst loading as mentioned in Table 1. The TOF value of Ni_3Se_2 was calculated to be 0.044 s^{-1}, which is higher than the previously reported TOF values for some Ni-based catalysts[7] , and is also roughly 5-fold higher than that of the reported IrOx (0.0089 s^{-1}) catalyst,[7] indicating a better OER activity for Ni_3Se_2.

Stability of the Ni_3Se_2 electrocatalyst under conditions of continuous oxygen evolution was investigated through chronoamperometric measurements (*j* vs *t*) at a overpotential where current density was around 10 mA/cm^2 in 0.3 M KOH for 18 h and 42 h and shown in inset of Fig 6 (b) and Fig. S9 (a), respectively. The onset potentials for the catalysts were measured in solutions which were not agitated. However, it was observed that as the electrochemical O_2 generation proceeded, there was large amount of bubble formation most of which adhered to the surface of the catalyst, thereby slowing down the reaction. Hence, for studies including long-term stability the solution was stirred with minimal speed (upto 300 rpm) to dislodge the bubbles from the catalyst surface and allow progress of the reaction. Structural and compositional stability of the films after extended periods of oxygen evolution (18 and 42 h at room temperature) was also studied through powder X-ray diffraction, XPS and LSV analyses (Figure 6). All catalysts exhibit excellent stability over extended periods of time. The LSV curves after 18 h of continuous O2 evolution showed similar onset potential and overpotential at 10 mA/cm^2 with very minimal difference in the current density for OER activities as compared with the initial catalyst (Figure 6a). Pxrd showed that the structural integrity was maintained even after 42 h of catalytic activity with no obvious sample degradation (Figure 6d). XPS spectra showed that the elemental composition was maintained after extended periods of catalytic activity (Figure 6c). In contrast to Ni_3S_2 report where the XPS data after OER activity showed complete depletion of the Ni_3S_2 layer on the surface,[34] in the present case, the catalyst after OER activity still showed major presence of Se on the surface. The O 1s and Se 3d signal before and after OER activity showed minimal change (Supplementary figure S7). Raman studies also indicated that the catalyst after OER activity was still Ni_3Se_2 and the characteristic peaks for Ni-oxide or hydroxide were not visible (Figure 6e). The long-term stability was also investigated from Raman studies performed on the Ni_3Se_2 catalyst after 18 h of continuous O_2 evolution, which still showed a similar spectra with marked absence of peaks characteristic of Ni-based oxide and/or hydroxide (supplementary figure S8). However the films after catalytic activity showed lesser Se content compared to the pristine films, indicating that the Ni_3Se_2 films might be getting more Se deficient with prolonged catalytic activity.

Interestingly, the LSV curves after 42 h of continuous OER, showed that the catalyst became even more efficient

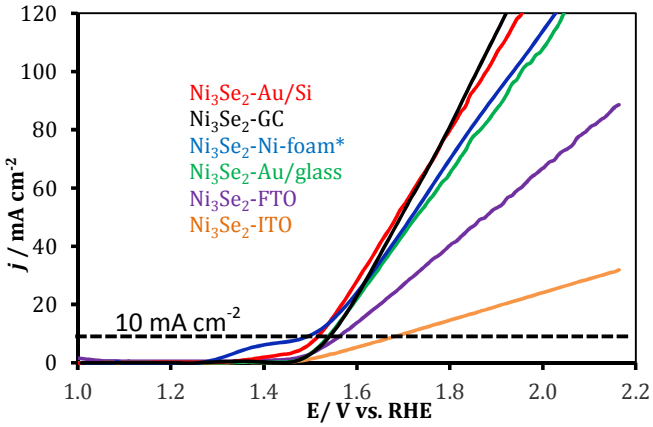

Fig. 8 OER activities of Ni_3Se_2 catalysts electrodeposited on various substrates. * - the geometric area of the catalyst was estimated from the area exposed to the electrolyte not considering the surface area of the Ni foam.

Table 2: Comparison of the η (onset and at 10 mA/cm^2 with Ni_3Se_2 deposited on different substrates.

Ni_3Se_2@ different Substrate	Onset overpotential, η, V/ vs. RHE	Overpotential,V/vs. RHE to achieve current 10 mA/cm^2
Au-Si	0.210	0.300 ± 0.10
GC	0.220	0.310 ± 0.20
Au-glass	0.220	0.320 ± 0.20
Ni-foam	0.230	0.270 ± 0.20
FTO	0.240	0.340 ± 0.20
ITO	0.250	0.450 ± 0.30

after such prolonged activity (η = 310 mV at 10 mA/cm^2) (Supplementary Figure S9a) while maintaining similar composition and structure (Figures 6 (c) and 6 (d)). Improved catalytic efficiency with aging has been observed in Ni-oxide and hydroxide based catalysts before[7,65] and this has been attributed due to several factors including structural modification of the films. Some observations also suggested that prolonged aging (for several weeks) in impure KOH without potential cycling, led to Fe incorporation in the films from the reagent grade KOH which contains ~0.66 ppm of Fe as impurity.[65,66] Hence, we have analyzed the catalytic composition through ICP-MS studies after 42 h of continuous OER activity in alkaline medium. The ICP-MS studies revealed that there was trace amount of Fe incorporation [Ni:Fe approximately 1:0.015] from the unpurified KOH upon extended exposure. In Boettcher's paper the authors have also suggested a way of purifying the KOH to be Fe-free by treatment with precipitated $Ni(OH)_2$.[65] Accordingly, we have also carried out similar treatment to the KOH electrolyte to generate a Fe-free solution, which was then tested with the Ni_3Se_2 films for OER activity. The effect of Fe incorporation was studied through cycling studies where the catalysts were cycled in purified and unpurified KOH for 100 runs and the LSV curves were compared. It was observed that in case of unpurified KOH, the current density increased slightly with increasing number of cycles, while for purified KOH the current density (at high potential) decreased slightly with increasing cycles (Supplementary Figure S9b). Hence it can be concluded that like the Ni-oxyhydroxide based catalysts, in this case also Fe incorporation in the catalyst composition is possible and the catalytic activity can be enhanced through such doping. Taking cue from these observations including the ICP-MS data and research reported by Boettcher's group,[54,55] we are attempting to intentionally incorporate Fe in these Ni-selenide based films and investigate their catalytic activities towards OER process.[67]

Effect of Annealing. Thermal annealing is considered to be an effective way to improve the activity of catalyst.[68] Figure 7 shows the LSVs of Ni_3Se_2 catalyst before and after annealing at 300 °C for 5 min on hot plate as well as in a horizontal oven (30 min) under controlled flow of N_2 in either case. The OER activity of the catalyst improved significantly after the heat treatment, the current density of 10 mA cm^{-2} was achieved at an overpotential of 290 mV in 0.3 M KOH. Structural, morphological and spectral analysis of the annealed films revealed that: (i) annealing at 300 °C does not affect the surface morphology of catalyst (Supporting SEM images shown in figure S10); (ii) however the crystallinity of catalyst improved significantly which was evidenced by pxrd (Supporting figure S11); (iii) ratio of Ni to Se increases with the thermal treatment which was evident from EDS (Supplementary table, ST1). Structurally enhanced more Se-deficient films formed through annealing may provide more active sites for OER, thus leading to better catalytic activity.

Effect of Substrate on OER Activities. Besides Au-glass and Au-coated Si, GC, ITO, FTO-coated glass and Ni-foam were also used as underlying substrate to investigate the effect of substrate on OER. The LSVs of the respective electrocatalysts have been shown in Figure 8. The overpotentials required to achieve 10 mA/cm^2 for the catalyst deposited for 300 s on various substrate are presented in Table 2. The catalyst deposited on Au-coated glass and Si substrates as well as GC exhibited highest current density and earliest onset of OER as compared with others. This observation suggests that the interaction between underlying substrate and Ni_3Se_2 may play role on the OER activity. The effect of substrate on OER activity has been previously reported in the literature for Ni-based catalysts.[10] In addition to planar substrates, Ni_3Se_2 films were also electrodeposited directly into high surface area Ni foam. The LSV plots of Ni_3Se_2-Ni foam composite exhibited the lowest onset overpotential for OER at 230 mV (*vs* RHE) as shown Figure 8. The overpotential at 10 mA/cm^2 for Ni_3Se_2-Ni foam composite was also the lowest in the series (270 mV *vs* RHE). However, the Ni foam being exceptionally porous with very high surface area, it may not be judicial to use the geometric surface area of the electrode to estimate the current density, and compare it with the planar substrates. Nevertheless, the high surface area of the foam makes sure that the entire Ni_3Se_2 catalyst is accessible to the electrolyte thereby can potentially significantly enhance the catalytic efficiency.

Conclusions

A nickel selenide based compound, Ni_3Se_2 with structure analogous to mineral *Heazlewoodite* has been observed to be catalytically active towards OER in alkaline medium (pH = 13) for the first time. The low onset overpotential required for O_2 evolution as well as low overpotential required to reach 10 mA/cm^2, gives this catalyst a very competitive edge amongst the known oxide based OER electrocatalysts. A comparison with other reported Ni-based OER catalyst (Table 3) revealed that the Ni_3Se_2 system described in this paper is definitely as good as or even better than the best Ni-based OER catalyst. Moreover, this Se-deficient phase containing a rich architecture of metal-metal bond can be further modified through solid state chemistry approaches to optimize the catalytic efficiency. These Ni_3Se_2 catalysts electrodeposited on conducting substrates, also exhibited exceptional stability under the conditions of O_2 evolution for extended periods of time. These findings coupled with the simple synthesis method, earth-abundancy of the raw materials and

Table 3: Comparison of the catalytic performances between different Ni-based catalyst and Ni_3Se_2.

Catalyst	Onset Overpotential (V), η (vs. RHE)	Overpotential (V), η (vs. RHE) required to get 10 mA cm^{-2}	Tafel slope, (mV dec^{-1})	Reference
IrOx	-	0.32		9
[c]RuO_2	0.22*	0.39*	-	16
[a]NFNTAs-20	0.28	0.38 (to get 5 mA cm^{-2})	105	27
[b]NNCNTAs	0.31	0.46	65	28
α-$Ni(OH)_2$	0.310*	0.331	42	26
Ni_3S_2-Ni foam	0.157	0.187	159.3	34
$NiCo_2O_4$	0.260*	0.34	75	60
$Ni_{0.9}Fe_{0.1}O_x$	0.250*	0.336	30	7,65
NiCo-LDH	0.290	0.410*	-	29
Ni_3Se_2-Au@Glass	0.220	0.320 ± 0.20	97.1	This Work
Ni_3Se_2-Au@Glass (Annealed)	0.210	0.290 ± 0.10	97.2	This Work
Ni_3Se_2-Au@Si	0.210	0.300 ± 0.10	122.0	This Work
Ni_3Se_2-GC	0.220	0.310 ± 0.20	79.5	This Work
Ni_3Se_2-Ni foam	0.230	0.270 ± 0.20	142.8	This Work

[a] Ni-Fe oxide nanotube arrays (20% of Fe)
[b] Ni@$[Ni^{(2+/3+)}Co_2(OH)_{6-7}]_x$ nanotube arrays
[c] In acidic electrolyte
* Estimated from the references

possibilities to tune the catalytic efficiencies even further, makes them lucrative for various energy-related practical applications.

Acknowledgements

MN would like to acknowledge American Chemical Society Petroleum Research Fund (54793-ND10) for financial support. The authors would also like to acknowledge CS3M at Missouri S&T, Dr. Honglan Shi and Kun Liu for help with the ICP-MS measurements, Materials Research Center for equipment usage and Dr. Richard Brow for help with Raman measurements.

Notes and references

‡ The Ni_3Se_2 crystal can be described as formed by anion (Se) close packing and Ni occupying 3/4th of the tetrahedral holes. Ni sits in a distorted tetrahedral coordination of Se, while Se sits within a distorted trigonal prismatic coordination formed by the neighbouring Ni atoms. Since large number of the tetrahedral holes has been occupied by Ni, the neighbouring Ni polyhedra have edge-sharing bringing the Ni atoms close together favouring formation of the metal-metal bond.

1 N. S. Lewis and D. G. Nocera, *Proc. Natl. Acad. Sci. U. S. A.*, 2006, **103**, 15729–15735.
2 M. G. Walter, E. L. Warren, J. R. McKone, S. W. Boettcher, Q. Mi, E. A. Santori and N. S. Lewis. Solar Water Splitting Cells. *Chem. Rev*., 2010, **110**, 6446–6473.
3 T. R. Cook, D. K. Dogutan, S. Y. Reece, Y. Surendranath, T. S. Teets and D. G. Nocera, *Chem. Rev*., 2010, **110**, 6474–6502.
4 J. O. Bockris and A. K. N. Reddy, Modern Electrochemistry 1: Ionics, Plenum Press, New York, 1998.
5 W. T. Hong, M. Risch, K. A. Stoerzinger, A. Grimaud, J. Sunitvich and Y. S. Horn, *Energy Energy Environ. Sci.,* 2015, **8**, 1404.
6 L. Trotochaud and S. W. Boettcher, *Scripta Materialia,* 2014, **74**, 25-32.
7 L. Trotochaud, J. K. Ranney, K. N. Williams and S. W. Boettcher, *J. Am. Chem. Soc.,* 2012, **134**, 17253-17261.
8 G. M. Whitesides and G. W. Crabtree, *Science,* 2007, **315**, 796-798.
9 C. C. L. McCrory, S. Jung, J. C. Peters, and T. F. Jaramillo, *J. Am. Chem. Soc*., 2013, **135**, 16977-16987.
10 (a) E. Fabbri, A. Habereder, K. Waltar, R. Kotz and T. J. Schmidt, *Catal. Sci. Technol.,* 2014, **4**, 3800-3821; (b) J. Qi, X. Lai, J. Wang, H. Tang, H. Ren, Y. Yang, Q. Jin, L. Zhang, R. Yu, G. Ma, Z. Su, H. Zhao, and D. Wang, *Chem. Soc. Rev.*, 2015, DOI: 10.1039/c5cs00344j. (c) H. Tang, C. M. Hessel, J. Wang, N. Yang, R. Yu, H. Zhao, and D. Wang, *Chem. Soc. Rev.* 2014, **43**, 4281.
11 J. Suntivich, K. J. May, H. A. Gasteiger, J. B. Goodenough and Y. S. Horn, *Science*, 2011, **334**, 1383-1385.
12 S. W. Lee, C. Carlton, M. Risch, Y. Surendranath, S. Chen, S. Furutsuki, A. Yamada, D. G. Nocera, and Y. S. Horn*, J. Am. Chem. Soc.*, 2012, **134**, 16959-16962.
13 E. Mirzakulova, R. Khatmullin, J. Walpita, T. Corrigan, N. M. Vargas-Barbosa, S. Vyas, S. Oottikkal, S. F. Manzer, C. M. Hadad, and K. D. Glusac, *Nature Chem*., 2012, **4**, 794-801.
14 X. Li, F. Walsha and D. Pletcher, *Phys. Chem. Chem. Phys.,* 2011, **13**, 1162-1167.
15 J. Rossmeisl, Z. W. Qu, H. Zhu, G. J. Kroes and J. K. J. Norskov, *Electroanalytical Chemistr*y, 2007, **607**, 83-89.

16 Y. Lee, J. Suntivich, K. J. May, E. E. Perry and Y. S. Horn, *J. Phys. Chem. Lett*., 2012, **3**, 399-404.
17 M. Gong and H. Dai, *Nano Research,* 2015, **8**, 23-39.
18 H. N. Seiger and R. C. Shair, *J. Electrochem. Soc.,* 1961, **108**, C163-C163.
19 Y. G. Li, P. Hasin and Y. Y. Wu, *Adv. Mater.,* 2010, **22**, 1926-1929.
20 G. P. Gardner, Y. B. Go, D. M. Robinson, P. F. Smith, J. Hadermann, A. Abakumov, M. Greenblatt and G. C. Dismukes, *Angew. Chem., Int. Ed*., 2012, **51**, 1616-1619.
21 J. Landon, E. Demeter, N. Inoglu, C. Keturakis, I. E. Wachs, R. Vasic, A. I. Frenkel and J. R. Kitchin, *ACS Catal*., 2012, **2**, 1793-1801.
22 M. Gong, Y. G. Li, H. L. Wang, Y. Y. Liang, Y. Y. and J. Z. Wu, J. G. Zhou, J. Wang, T. Regier, F. Wei, and H. J. Dai, *J. Am. Chem. Soc*., 2013, **135**, 8452-8455.
23 S. Chen and S. Z. Qiao, *ACS Nano*, 2013, **7**, 10190-10196.
24 S. Chen, J. J. Duan, M. Jaroniec and S. Z. Qiao, *Angew. Chem. Int. Ed.,* 2013, **52**, 13567-13567.
25 M. R. Gao, Y. F. Xu, J. Jiang, Y. R. Zheng and S. H. Yu, *J. Am. Chem. Soc*., 2012, **134**, 2930-2933.
26 M. Gao, W. Sheng, Z. Zhuang, Q. Fang, S. Gu, J. Jiang, and Y. Yan, *J. Am. Chem. Soc*., 2014, **136**, 7077-7084.
27 Z. Zhao, H. Wu, H. He, X. Xu and Y. Jin, *J. Mater. Chem. A*, 2015, **3**, 7179-7186.
28 Z. Zhao, H. Wu, H. He, X. Xu, and Y. Jin, *Adv. Funct.Mater*. 2014, **24**, 4698–4705.
29 J. Jiang, A. Zhang, L. Li, and L. Ai, *J. of Power Sources*, 2015, **278**, 445-451.
30 M. R. Gao, Y. F. Xu, J. Jiang, and S. H. Yu, *Chem. Soc. Rev,*.2013*,* **42**, 2986-3017.
31 M. D. Merrill and R. C. Dougherty, *J. Phys. Chem. C,* 2008, **112,** 3655-3666.
32 W. Xu, Z. Lu, X. Lei, Y. Li and X. Sun, *Phys. Chem. Chem. Phys.,* 2014, **16**, 20402-20405.
33 Q. Liu, J. Shi, J. Hu, A. M. Asiri, Y. Luo and X. Sun, *ACS Appl. Mater. Interfaces,* 2015, **7**, 3877-3881.
34 W. Zhou, X. J. Wu, X. Cao, X. Huang, C. Tan, J. Tian, H. Liu, J. Wang and H. Zhang, *Energy Environ. Sci.*, 2013, **6**, 2921-2924.
35 H. Yuan, H. Wang and Y. Cui, *Acc. Chem. Res.,* 2015, **48**, 81-90.
36 F. C. Hsu, J. Y. Luo, K. W. Yeh, T. K. Chen, T. W. Huang, P. M. Wu, Y. C. Lee, Y. L. Huang, Y. Y. Chu, D. C. Yan and M. K. Wu, *Proc. Natl. Acad. Sci. USA*, 2008, **105**, 14262-14264.
37 N. C. Gresty, Y. Takabayashi, A. Y. Ganin, W. T. McDonald, J. B. Claridge, D. Giap, Y. Mizuguchi, Y. Takano, T. Kagayama, Y. Ohishi, M. Takata, M. J. Rosseinsky, S. Margadonna and K.Prassides, *J. Am. Chem. Soc.,* 2009, **131**, 16944-16952.
38 J. Puthussery, S. Seefeld, N. Berry, M. Gibbs, and M. Law, *J. Am. Chem. Soc.*, 2011, 133, 716-719.
39 F. Cao, R.X. Liu, L. Zhou, S.Y. Song, Y. Q. Lei, W.D. Shi, F.Y. Zhao, and H. J. Zhang, *J. Mater. Chem.*, 2010, **20**, 1078-1085.
40 M. R. Gao, Q. Gao, J. Jiang, C. H. Cui, W. T. Yao and S. H. Yu, *Angew. Chem. Int. Ed*., 2011, 50, 4905-4908.
41 M. R. Gao, R. S. Liu, J. Jiang, C. H. Cui, W. T. Yao and S. H. Yu, *J. Mater. Chem.*, 2010, **20**, 9355-9361.
42 M. R. Gao, Z. Y. Lin, T. T. Zhuang, J. Jiang, Y. F. Xu, Y. R. Zheng and S. H. Yu, *J. Mater. Chem*., 2012, **22**, 13662-13668.
43 R. A. Sidik and A. B. Anderson, *J. Phys. Chem. B*, 2006, 110, 936-941.
44 L. Zhu, D. Susac, M. Teo, K. C. Wong, P. C. Wong, R. R. Parsons, D. Bizzotto and K. A. R Mitchell, *J. Catal.*, 2008, **258**, 235-242.
45 Y. X. Zhou, H. B. Yao, Y. Wang, H. L. Liu, M. R. Gao, P. K. Shen and S. H. Yu, *Chem. Eur., J.* 2010, **16**, 12000-12007.
46 Y. G. Feng, T. He and N. Alonso-Vante, *Chem. Mater.*, 2008, **20**, 26-28.
47 E. Vayner, R. A. Sidik, A. B. Anderson and B. N. Popov, *J. Phys. Chem.*, 2007, **111**, 10508-10513.
48 Y. J. Feng, T. He, N. Alonso-Vante, *Electrochim. Acta*, 2009, **54**, 5252-5256.
49 G. Wu, G. F Cui, D. Y. Li, P. K. Shen and N. Li, *J. Mater. Chem.,* 2009, **19**, 6581-6589.
50 J. B. Parise, *Acta Crystallogr.,* 1980, **36**, 1179-1180.
51 M. E. Fleet, *American Mineral.,* 1977, **62**, 341-345.
52 R. P. Agarwala and A. P. B. Sinha, *Z. Anorg. Allg. Chem.,* 1957, **289**, 203-206.
53 J. P. Rouche and P. Lecocq *Comptes Rendus Chemie.,* 1966, **262**, 555.
54 G. V. Gibbs, R. T. Downs, C. T. Prewitt, K. M. Rosso, N. L. Ross and D. F. Cox, *J. Phys. Chem. B*, 2005, **109**, 21788-21795.
55 Z. Loizos and N. Spyrellis, *Thin Solid Films***,** 1991, **204**, 139-149.
56 I. M. Sadiek, A. M. Mohammad, M E. El-Shakre, M. I. Awad, M. S. El-Deab and B. E. El-Anadouli, *Int. J. Electrochem. Sci*., 2012**, 7**, 3350-3361.
57 R. B. Shalvoy and P. J. Reucroft, *J. Vac. Sci. Technol.,* 1979, **16**, 567.
58 Y. Liao, K. Pan, Q. Pan, G. Wang, W. Zhou and H. Fu, *Nanoscale*, 2015, **7**, 1623-1626.
59 W. Shi, X. Zhang and G. Chen, *Int. J. Hydrogen Energy,* 2013, **38**, 7037-7045.
60 X. Lv, Y. Zhu, H. Jiang, X. Yang, Y. Liu, Y. Su, J. Huang, Y. Yao and C. Li, *Dalton Trans.*, 2015, **44**, 4148-4154.
61 A. B. Mandale, S. Badrinarayanan, S. K. Date and A. P. B. Sinha, *J. Electron. Spectrosc. Relat. Phenom.,* 1984, **33**, 61.
62 C. E. M. Camposa, J. C. de Limaa, T. A. Grandia, K. D. Machadoa, P.S. Pizanib and R. Hinrichs, *Solid State Ionics*, 2004, **168**, 205-210.
63 J. Ran, J. Zhang, J. Yu, M. Jaroniec and S. Z. Qiao. *Chem. Soc. Rev*., 2014, **43**, 7787-7812.
64 Qiu, Y.; Xin, L.; Li, W. *Langmuir*, **2014**, *30*, 7893-7901.
65 L. Trotochaud, S. L. Young, J. K. Ranney, and S. W. Boettcher, J. Am. Chem. Soc. 2014, **136**, 6744-6753.
66 D. Corrigan, *A. J. Electrochem. Soc*., 1987, **134**, 377-384.
67 A. Swesi, J. Masud, M. Nath *unpublished results*.
68 J. Masud, T. V. Nguyen, N. Singh, E. McFarland, M. Ikenberry, K. Hohn, C. J. Pan and B. J. Hwang *J. Electrochem. Soc.,* 2015, **162**, F455-F462.

Nickel Selenide As High-efficiency Catalyst for Oxygen Evolution Reaction

A. T. Swesi,[§] J. Masud[§] and M. Nath*

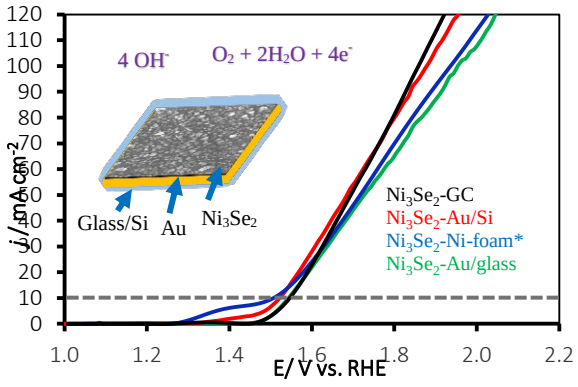

Ni_3Se_2 has been identified as a high-efficiency oxygen evolution catalyst with low onset potential and extended stability in alkaline conditions.

Nickel Selenide As High-efficiency Catalyst for Oxygen Evolution Reaction

A. T. Swesi, J. Masud and M. Nath*

Broader Context:

Oxygen evolution is one of the most kinetically hindered process for water electrolysis. Thus, oxygen evolution catalysts containing earth abundant elements have recently been at the center of attraction to address this challenge both in terms of high performance and practical applicability. Nickel oxides are among the best precious metal-free commercial electrolyzers. However, replacing the oxides with selenides introduces several favorable factors which can further enhance the catalytic performance of the nickel based electrocatalysts. This article describes the identification of Ni_3Se_2 as high-efficiency oxygen evolution electrocatalyst with extended stability under alkaline conditions capable of generating oxygen at a much lower applied potential. Structural richness of the chalcogenides along with their amenable electronic property holds a lot of promise for further tuning of the electrocatalyst performance and systematic studies with the nickel chalcogenides will significantly benefit the search for a water oxidation catalyst with low cost, high-efficiency and high durability.